PROCEEDINGS OF SPIE

SPIEDigitalLibrary.org/conference-proceedings-of-spie

Zn-vacancy related defects in ZnO grown by pulsed laser deposition

F. C. C. Ling
C. Q. Luo
Z. L. Wang
W. Anwand
A. Wagner

SPIE.

Downloaded From: https://www.spiedigitallibrary.org/conference-proceedings-of-spie on 8/16/2017 Terms of Use: https://spiedigitallibrary.spie.org/ss/TermsOfUse.aspx

Zn-vacancy related defects in ZnO grown by pulsed laser deposition

F. C. C. Ling[1,*], C. Q. Luo[1], Z. L. Wang[1], W. Anwand[2], A. Wagner[2]
[1] Department of Physics, The University of Hong Kong, Pokfulam, China; [2] Institute of Radiation Physics, Helmholtz-Zentrum Dresden-Rossendorf, Bautzner Landstr. 400, 01328 Dresden, Germany

*ccling@hku.hk

ABSTRACT

Undoped and Ga-doped ZnO (002) films were grown c-sapphire using the pulsed laser deposition (PLD) method. Zn-vacancy related defects in the films were studied by different positron annihilation spectroscopy (PAS). These included Doppler broadening spectroscopy (DBS) employing a continuous monenergetic positron beam, and positron lifetime spectroscopy using a pulsed monoenergetic positron beam attached to an electron linear accelerator. Two kinds of Zn-vacancy related defects namely a monovacancy and a divacancy were identified in the films. In as-grown undoped samples grown with relatively low oxygen pressure $P(O_2) \leq 1.3$ Pa, monovacancy is the dominant Zn-vacancy related defect. Annealing these samples at 900 ^oC induced Zn out-diffusion into the substrate and converted the monovacancy to divacancy. For the undoped samples grown with high $P(O_2)=5$ Pa irrespective of the annealing temperature and the as-grown degenerate Ga-doped sample ($n \approx 10^{20}$ cm^{-3}), divacancy is the dominant Zn-vacancy related defect. The clustering of vacancy will be discussed.

Keywords: ZnO; pulsed laser deposition; positron annihilation spectroscopy; Zn-vacancy related defects; monovacancy; divacancy

1. INTRODUCTION

ZnO is a functional oxide material having a variety of applications, including optoelectronic, spintronic, sensors, transparent electronic, photovoltaic, photocatalysis, etc [1]. For the optoelectronic applications, ZnO has a direct wide band gap ($\approx$3.2 eV at room temperature) and a large exciton binding energy ($\approx$60 meV). Its exciton binding energy is significantly larger than another widely used direct wide band gap semiconductor GaN (25 meV), and thus exciton process emission is feasible at room temperature for ZnO. These make ZnO a good potential choice for fabricating ultra-violet devices like diode laser, light emitting diode (LED) or solid state white lighting device [1]. For example, a very low lasing threshold of 6 $kWcm^{-2}$ was achieved in an optical pumping study on asymmetric double quantum well (ADQW) ZnO/ZnMgO structure [2]. Group III element doped ZnO is also a good material for transparent electrode because of its low resistivity and high optical transmittance, as well as its non-toxicity, abundance in earth availability and low-cost (for examples references [3-5]).

Despite of the excellent physical parameters for fabricating UV optoelectronic devices, the development of practical ZnO-based devices is hindered by the asymmetric p-type doping difficulty [6,7], which was associated with the formation of compensating defects, the low solubility of the p-type dopant, and the low solubility of the dopant, and the large ionization energy of the acceptor [7]. Recent results showed that the involved shallow acceptors yielded from the p-type doping were usually defect complexes comprising of the intrinsic defect rather than the simple dopant substitution defect [8-11]. This implies that the exact knowledge of the intrinsic defects and their control in ZnO is essential for the controlled formation of the desired shallow acceptor complex during the growth process. For the n^+-doping with Group III element like Ga, the intrinsic defects play crucial role in compensating the materials. It was experimentally found that the formations of acceptor defect complex comprising of Ga_{Zn} and the intrinsic defects (like Ga_{Zn}-V_{Zn} and Ga_{Zn}-O_i) [12], and the extra-high concentration of V_{Zn} induced by self-compensation [13] had the effect of suppressing the carrier and mobility. Other than the electrical properties, the intrinsic defects in ZnO also play important role in influencing the materials optical [14,15] and magnetic properties [16,17]. A review on the studies of defects in ZnO was given in reference [18].

Oxide-based Materials and Devices VIII, edited by Ferechteh H. Teherani, David C. Look,
David J. Rogers, Ivan Bozovic. Proc. of SPIE Vol. 10105, 101050F · © 2017 SPIE
CCC code: 0277-786X/17/$18 · doi: 10.1117/12.2267186

Downloaded From: https://www.spiedigitallibrary.org/conference-proceedings-of-spie on 8/16/2017 Terms of Use: https://spiedigitallibrary.spie.org/ss/TermsOfUse.aspx

Isolated Zn-vacancy defect V_{Zn} is a doubly ionized acceptor having two states (namely (0/-) and (-/2-)) in the band gap [19]. V_{Zn} was experimentally found to be the dominant acceptors in the as-grown undoped ZnO single crystal [20] and was the important compensating defect. V_{Zn} forms defect complexes with impurities in ZnO. For example, theoretical study showed that X_{Zn}-$(V_{Zn})_2$ (where X=P, As and Sb) were shallow acceptor and X_{Zn} was donor [10], and X_{Zn}-$(V_{Zn})_2$ was attributed to the observed p-type conductivity observed in P-doped and As-doped ZnO [11]. Zn-vacancy also formed complex with hydrogen [21,22], for which the V_{Zn}-2H was electrically inactive. Positron annihilation spectroscopy (PAS) is a non-destructive probe for neutral or negatively charged vacancy type defects in semiconductors [23,24]. After positron is implanted into the solid, it will be rapidly thermalized and then undergo diffusion in the delocalized state. As vacancy is the missing-out of a positively charged core atom, it is a potential well for the positron and thus the delocalized could be trapped by such vacancy. The positron in the solid will finally annihilate with a surrounding electron, either from the delocalized state or the localized defect state. The principal of PAS is that the outgoing annihilation gamma photons carry the information of the electronic structure around the annihilating positron-electron pair, and thus the PAS spectroscopic signals can be served as the fingerprints for the delocalized bulk state and the different vacancy states. For the case of ZnO, PAS is selectively sensitive to Zn-vacancy related defects. There have been relatively more PAS studies on the ZnO single crystals [20,22,25-29] and several on ZnO nanostructures [15,30] to identify the V_{Zn}-related defects and their thermal evolutions in these materials. Although device applications usually involve the use of ZnO materials in the form of thin films deposited on substrates, PAS studies on ZnO thin films are relatively few [31-34] and the understanding of V_{Zn}-related in ZnO films is far from complete.

In the present study, the Zn-vacancy-related defects in ZnO films grown by pulsed laser deposition (PLD) were studied by PAS. The Doppler broadening spectrum and the positron lifetime spectrum respectively reveal the electronic momentum distribution and the electronic density of the V_{Zn}-related defects in the ZnO films. Two kinds of V_{Zn}-related defects VZn1 and VZn2 were identified in undoped ZnO films, and their dominancy dependence on the stoichiometry during growth and post-growth annealing were investigated. The microstructures of VZn1 and VZn2 were also investigated.

2. EXPERIMENTAL

The ZnO films were grown on c-sapphire substrate using the PLD method with a background pressure of 10^{-4} Pa. The oxygen pressure during growth was systemically varied at $P(O_2)$= 0 Pa, 1 Pa, and 5 Pa. The laser pulse (wavelength of 248 nm) having the pulse energy of 300 mJ and repetition rate of 2 Hz from the Coherent COMPexPro 102 excimer laser was used for the growth. The substrate temperature was kept at 600 ^{o}C during the growth. Undoped, Ga-doped, and Cu-doped ZnO films were grown. The isochronal annealing was performed in a tube furnace in Ar-atmosphere for 40 minutes.

The Doppler broadening measurement [23.24] was carried out at room temperature using a 25 keV continuous monoenergetic positron beam as the positron source. The annihilation gamma ray energy spectrum was collected using a high purity Ge detector and the associated nuclear electronics, which had a full width half maximum of 1.3 keV for the 514 keV gamma photon line. The Doppler broadening of the line shape of the annihilation gamma photon peak was monitored by the S-parameter and W-parameter, which were respectively defined as the central window count and the sum of the two wing windows counts to the total count of the annihilation peak [23,24]. The central window for the S-parameter was set at 511±0.76 keV, and the wing windows were taken as 511+3.4 keV to 511+6.8 keV and 511-3.4 keV to 511-6.8 keV. The positron lifetime measurements on the film samples were conducted using the pulsed monoenergetic positron beam MePS with its detailed description given in reference [35]. The timing resolution of the system was 257 ps and each of the positron lifetime spectra contained 3×10^6 counts.

3. RESULTS AND DISCUSSIONS

The X-ray diffraction spectra of all the samples were similar that only ZnO (002) at ~34.3^{o}-34.6^{o}, sapphire (006) at ~41.7^{o} and ZnO (004) at ~72.1^{o} were found in the spectra. This shows that the as-grown ZnO films had the single-phase wurtzite structure with the c-axis as the preferential orientation. The peak positions and the corresponding FWHM's of the ZnO (002) as found in the XRD spectra of the undoped ZnO samples and Cu-doped ZnO samples (Cu weight ratio of 2 % and 4 %) grown with different oxygen pressures are tabulated in Table I. The FWHM of the (002) XRD peaks for

Downloaded From: https://www.spiedigitallibrary.org/conference-proceedings-of-spie on 8/16/2017 Terms of Use: https://spiedigitallibrary.spie.org/ss/TermsOfUse.aspx

the undoped ZnO and the 2 % Cu-doped ZnO films grown are ~0.19° for the different oxygen growth pressures. The FWHM for the 4 % Cu-doped ZnO grown without oxygen increases to 0.23°, showing that the crystalline quality becomes worse as the Cu content increases to 4 %. The FWHM further increases with increasing oxygen pressure during growth to 0.28° while oxygen pressure reaches 1 Pa.

The carrier concentrations of the samples obtained by room temperature Hall measurements are tabulated in Table I. The electron concentrations of the undoped ZnO are nearly constant at 4-6×10^{18} cm^{-3} for all the oxygen growth pressures $P(O_2)$=0 to 1 Pa. For the as-grown Cu-doped ZnO samples, the electron concentrations are 10^{18}-10^{19} cm^{-3} for $P(O_2)$= 0 Pa. Unlike the undoped ZnO for which its electron concentration is independent of $P(O_2)$, the electron concentration for Cu-doped samples significantly decreased with increasing $P(O_2)$, respectively to 2×10^{17} cm^{-3} and 7×10^{16} cm^{-3} for the 2 % and 4 % Cu-doped samples. Thus for controlling the Cu content and the oxygen pressure, ZnO:Cu films with a wide range of electron concentrations from 10^{16}-10^{19} cm^{-3} can be obtained. For the Ga-doped and the Ga-Cu co-doped samples grown with $P(O_2)$=0.02 Pa, the electron concentrations are around 5×10^{20} cm^{-3}.

Table I The peak position and the FWHM of the (002) peak in the XRD spectra, and the electron concentrations of the undoped ZnO, Cu-doped ZnO (Cu=2 % and 4 % by weight), Ga-doped ZnO (Ga=1 % by weight) and Ga-Cu co-doped ZnO (Ga=1 % and Cu=2 % by weight) samples grown with different oxygen pressure.

	Oxygen Pressure (Pa)	Peak Position of ZnO (002)	FWHM	n (cm^{-3})
ZnO	0	34.49°	0.19°	6×10^{18}
	0.02	34.54°	0.18°	6×10^{18}
	1	34.57°	0.19°	4×10^{18}
ZnO:Cu(2%)	0	34.44°	0.19°	3×10^{19}
	0.02	34.56°	0.20°	9×10^{17}
	0.05	34.51°	0.20°	2×10^{17}
ZnO:Cu(4%)	0	34.34°	0.23°	3×10^{18}
	0.02	34.46°	0.24°	3×10^{17}
	0.05	34.47°	0.26°	1×10^{17}
	1	34.49°	0.28°	7×10^{16}
ZnO:Ga(1%)	0.02 Pa		0.20°	6×10^{20}
ZnO:Ga(1%):Cu(2%)	0.02 Pa	34.67°	0.21°	4×10^{20}

Figure 1 (a) and (b) respectively show the S-parameter and W-parameter plotted against the positron incident energy for the sapphire substrate, the undoped ZnO, Cu-doped ZnO and the Ga-doped ZnO samples are shown in Figure 1. The ZnO films were grown with $P(O_2)$=0.02 Pa. Positrons incident into the sample are rapidly thermally and then undergoes diffusion. The average positron implantation depth is given by $\bar{x} = AE^{1.6}/\rho$, where A=4.0 μg$cm^{-2}$$keV^{-1.6}$ and ρ is the material density. Some positrons would diffuse back to the implanting surface and annihilate in the surface state. The remaining positrons annihilate in the film respectively in the delocalized bulk state and the vacancy-defects states. The measured S-parameter (and so does the W-parameter) is the weighted contributions from the different annihilation states, i.e., $S(E) = f_{surf}(E)S_{surf} + f_b(E)S_b + \sum f_{di}(E)S_{di}$, where f_{surf}, f_b and f_{di} are the fractions of positrons annihilating in the surface state, delocalized bulk state and the states of the *i*-th vacancy defect respectively, and S_{surf}, S_b and S_{di} are the corresponding characteristic S-parameters. The S-E data of the sapphire decreased with increasing E and saturated at S≈0.49. A larger E resulted in a larger $\bar{x}$ thus less positrons diffusing back to the positron implanting surface and annihilate at the surface state. The resultant S-parameter decreased with increasing *E* as the S_{surf} was larger than annihilating in the film. The S-parameter finally saturated at large E as the positron implanted depth $\bar{x}$ is too deep to positron diffusing back to the surface, and the saturated value of the S-parameter refers to that of the sapphire substrate (i.e. $S = f_b S_b + \sum f_{di} S_{di}$ for f_{surf}=0).

Downloaded From: https://www.spiedigitallibrary.org/conference-proceedings-of-spie on 8/16/2017 Terms of Use: https://spiedigitallibrary.spie.org/ss/TermsOfUse.aspx

For the samples of the ZnO film on sapphire substrate, the observed S-parameter firstly decreased with increasing E, which referred to the reduced f_{surf}. The S-parameter then reached a plateau, which was associated with majority of the positrons annihilated in the ZnO film. Further increase of E resulted in some of the positrons annihilating in the sapphire substrate thus leasing to the decrease of the observed S-parameter. The saturation of S-parameter at S≈0.49, which was the S-parameter of the sapphire substrate, was associated with all of the positrons annihilating in the sapphire substrate as E is large enough. The corresponding mean implantation depth for E=5 keV is ~100 nm. As the ZnO film thickness is ~200-300 nm, majority of the positrons incident with E=5 keV annihilate in the film and this could also be confirmed from the plateaus seen in the S-E and W-E plots. The S- and W-parameters of the ZnO films were thus taken at E=5 keV from the corresponding S-E and W-E plots.

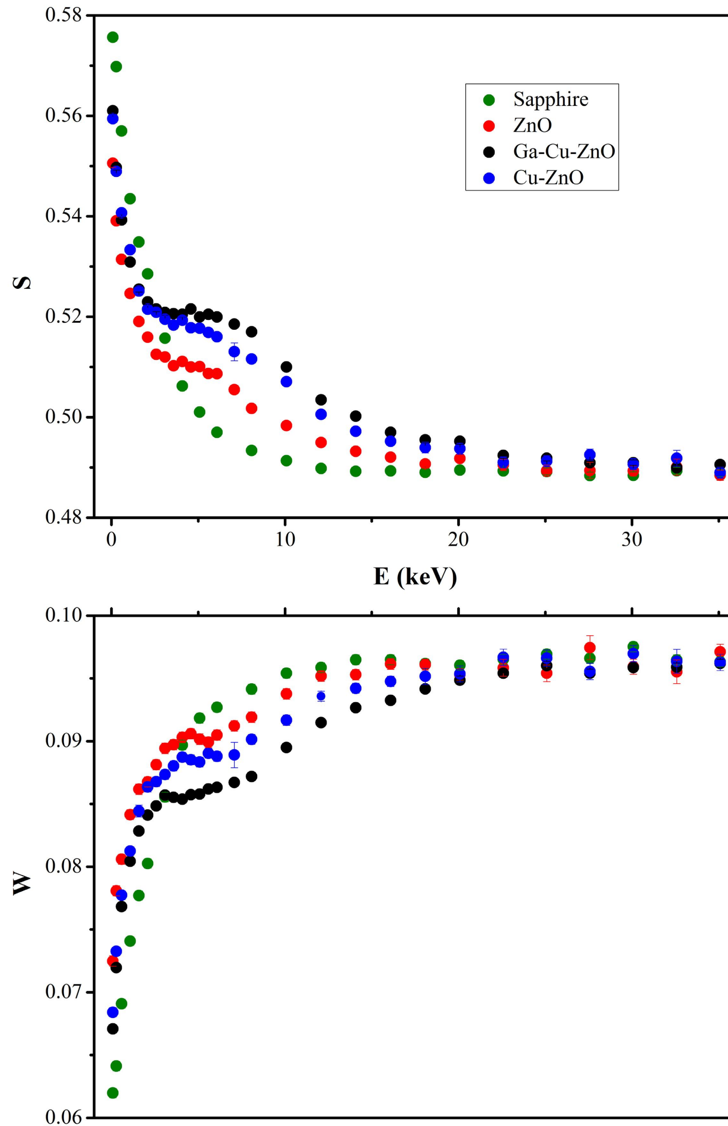

Figure 1 shows the (a) S-parameter; and (b) W-parameter against the positron incident energy for the sapphire substrate, the undoped ZnO film, Cu-doped, Ga-doped ZnO film, and Ga-Cu codoped ZnO film. All the ZnO films were grown on the sapphire substrate.

Downloaded From: https://www.spiedigitallibrary.org/conference-proceedings-of-spie on 8/16/2017 Terms of Use: https://spiedigitallibrary.spie.org/ss/TermsOfUse.aspx

The S- and W-parameters of the different ZnO films (obtained at E= 5keV) were shown in the S-W parameter plot in Figure 2. The S-W data of an annealed vacancy free ZnO single crystal is also included for reference. The resultant S-parameter (and also the W-parameter) is the contribution from the delocalized bulk state and vacancy defect states, i.e. $S = f_b S_b + \Sigma f_{di} S_{di}$. If a single type of defect exists, it can be worked out that $(S - S_b)/(W - W_b) = (S_d - S_b)/(W_d - W_b)$, implying that the corresponding S-W plot is a straight line. It is observed from Figure 2 that all the S-W data obtained from the ZnO films with different doping, oxygen growth pressure and post-growth annealing process are on two straight lines, namely VZn1 and VZn2. This implies that two kinds of Zn-vacancy related defects VZn1 and VZn2 with different microstructures are identified in these ZnO films grown by PLD. For the undoped ZnO samples grown with relatively low oxygen pressure, $P(O_2) \leq 1$ Pa, the samples were dominated by VZn1 with annealing temperatures below 900 ^oC, and converted to VZn2 as the annealing temperature reached 900 ^oC. For the undoped ZnO samples grown with relatively high oxygen pressure $P(O_2)=5$ Pa, the dominant Zn-vacancy related defect was VZn2 irrespective of the annealing temperature. These samples have $n \sim 10^{18}$-10^{19} cm^{-3}. For the as-grown Ga-doped and Ga-Cu co-doped ZnO samples which had $n \sim 10^{21}$ cm^{-3}, the dominant Zn-vacancy related defect was VZn2.

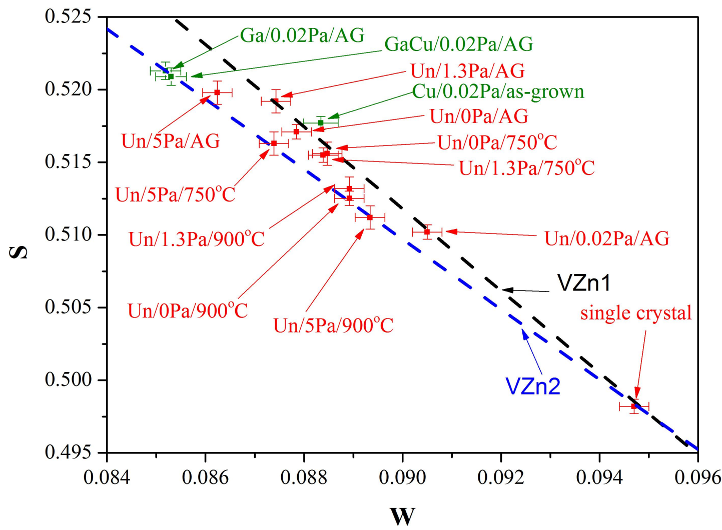

Figure 2 shows the S-W parameter plots of the ZnO samples.

Positron lifetime measurements were conducted on the as-grown undoped ZnO sample grown with $P(O_2)=1$ Pa and the as-grown Ga-doped ZnO sample grown with $P(O_2)=0.02$ Pa, for which their dominant Zn-vacancy related defects were respectively VZn1 and VZn2. The defect components of the undoped and Ga-doped ZnO had characteristic lifetime of 214 ps and 252 ps respectively. The S-E data (i.e. Figure 1) of these two samples were also fitted by the positron-diffusion-annihilation model using the source code VEPFIT [36], and their effective positron diffusion lengths were 12±0.6 nm and 7.1±0.3 nm, respectively (see Table II).

Table II The fitted characteristic lifetimes of the defect components $\tau_{exp,1}$ and the effective positron diffusion lengths L_+ of the undoped ZnO sample grown at $P(O_2)=0$ Pa and the Ga-doped ZnO sample grown with $P(O_2)=0.02$ Pa.

	$\tau_{exp,1}$	L_+
ZnO:Un, $P(O_2)=0$ Pa	214 ps	12±0.6 nm
ZnO:Ga(1%) $P(O_2)=0.02$ Pa	252 ps	7.1±0.3 nm

Downloaded From: https://www.spiedigitallibrary.org/conference-proceedings-of-spie on 8/16/2017 Terms of Use: https://spiedigitallibrary.spie.org/ss/TermsOfUse.aspx

The defect concentration were estimated from L_+ using the equation $C_V = \left[\left(L_{+,B}/L_+\right)^2 - 1\right] \Big/ \mu\tau_B$ [22], where $L_{+,B}$ is the positron diffusion length of the defect-free ZnO material, μ is the specific positron trapping coefficient and τ_B is the characteristic lifetime of the characteristic bulk lifetime. μ and τ_B had values of $\sim 3\times10^{15}$ ats^{-1} [37] and 151 ps [22] respectively. Typical values of L_+ for semiconductors are ~200 nm. However for the case of ZnO, the largest reported value of L_+ for ZnO single crystal was only ~70 nm. Nevertheless, the limits of the defect concentrations were found by putting in L_+ equal to 70 nm and 200 nm. These yielded the VZn1 concentration of 3×10^{18} to 3×10^{19} cm^{-3} in the as-grown undoped sample and the VZn2 concentration of 9×10^{18} to 8×10^{19} cm^{-3} in the Ga-doped sample. As saturated positron trapping into the defects is expected for defect concentration larger than 10^{18}-10^{19} cm^{-3}, there were saturated positron trappings into the VZn1 and VZn2 for the undoped and the Ga-doped ZnO samples respectively. This implies that VZn1 and VZn2 have the characteristic positron lifetimes of 214 ps and 252 ps respectively. As there have been reports of monovacancy V having lifetimes of 207 and 209 ps [38,39] and 230 ps [20,26], VZn1 is associated with the Zn monovacancy V_{Zn}. VZn2 was ascribed to divacancy $V_{Zn}V_O$ as there were previous reports of 257 ps for divacancy [38,39]. To conclude, V_{Zn} monovacancy dominated in the ZnO films grown with relatively low oxygen pressure ($P(O_2)$=0-1 Pa) and annealed at low temperatures ≤750 °C. For these samples, V_{Zn} monovacancy converted to $V_{Zn}V_O$ divacancy after annealing 900 °C, for which Zn out-diffusion into the substrate was simultaneously observed by SIMS [34]. All of the these samples (as-grown, annealed at 750 °C or 900 °C) have moderate electron concentration $\sim10^{18}$ cm^{-3}. For the Ga-doped and Ga-Cu co-doped ZnO samples which had high electron concentration $\sim10^{20}$ cm^{-3} and the undoped samples grown with high oxygen pressure $P(O_2)$=5 Pa, $V_{Zn}V_O$ divacancy was the dominant defect irrespectively of the annealing temperature.

Vacancy clustering is not an equilibrium process [40]. The dissociation energy barrier for the divacancy in ZnO is high (>2.5 eV). This implies once the divacancy is formed it is difficult to dissociate or anneal out, although its formation energy is lower than those for the other intrinsic defects like V_{Zn} or V_O. It is thus reasonable to postulate that annealing would favor the aggregation of V_{Zn} to form $V_{Zn}V_O$ rather than the annealing out of V_{Zn} if the V_{Zn} is above a threshold concentration. Studying the O-implanted ZnO using PAS, a threshold V_{Zn} concentration of 10^{19} cm^{-3} for vacancy clusterization was reported. This showed that the V_{Zn} concentration in the present undoped ZnO films grown with relatively low $P(O_2)$=1 Pa is close to this threshold concentration for clusterization. The thermal annealing behaviors of all the undoped samples grown with relatively low $P(O_2)$≤1 Pa were similar. The S-W data of the as-grown samples are all on the V_{Zn} line. Annealing at 750 °C decreased the S-parameter (increased the W-parameter) while the S-W data remained on the V_{Zn} line. This implied decrease of V_{Zn} concentrations but no change in the microstructure of the defect. Annealing these samples at 900 °C converted the V_{Zn} to $V_{Zn}V_O$. This could be due to the creation of the extra V_{Zn} left out from the Zn out-diffusion, and thus the kick-off of the V_{Zn} aggregation.

For the degenerate Ga-doped and Ga-Cu co-doped ZnO samples having high electron concentration $\sim10^{21}$ cm^{-3}, the Fermi level E_F is very close to or in the conduction band minimum (CBM). First-principal-calculation study on intrinsic defects in ZnO showed that the formation energy of V_{Zn} decreased as E_F moved towards the CBM [19]. This implied that the V_{Zn} concentration would be enhanced by the n^+-doping in ZnO, and this was known as the self-compensation [13]. Look et al [13] observed a Zn-vacancy concentration of $\sim10^{20}$ cm^{-3} with the $\sim10^{21}$ cm^{-3} Ga-doping in ZnO. Thus the V_{Zn} aggregation to form $V_{Zn}V_O$ in the present degenerate Ga-doped and Ga-Cu co-doped samples was associated with the high V_{Zn} concentration in these degenerate samples. For the present undoped ZnO grown in high oxygen pressure (i.e. $P(O_2)$=5 Pa), the dominancy of divacancy could also be associated to the lowering of the formation energy of V_{Zn} in the O-rich growth condition [19].

Undoped and Cu-doped ZnO samples grown by the similar PLD method have been studied by the coincidence Doppler broadening (CDB) spectroscopy [41]. The CDB spectrum revealed the longitudinal electronic momentum p_L distribution of the positron annihilation site, and was thus the fingerprint of the vacancy type defect. The CDB spectrum of the as-grown undoped ZnO sample grown at $P(O_2)$=0 Pa and substrate temperature of 300 °C (which was normalized to unity) was different from that annealed at 900 °C. This result agreed with the present findings that annealing at 900 °C changed the microstructure of the Zn-vacancy related defect from V_{Zn} to $V_{Zn}V_O$, thus also implying that the corresponding CDB spectra (i.e. the electronic momentum distribution) are the fingerprint defect spectra for V_{Zn} and $V_{Zn}V_O$. The CDB spectrum of the as-grown Cu-doped sample showed a negative characteristic peak at $p_L \sim 14\times10^3$ m_0c, where m_0 is the electron mass and c is the speed of light. This negative characteristic peak was also found in the CDB spectrum of the pure Cu sample. This characteristic negative peak in the as-grown Cu-doped ZnO sample was explained

Downloaded From: https://www.spiedigitallibrary.org/conference-proceedings-of-spie on 8/16/2017 Terms of Use: https://spiedigitallibrary.spie.org/ss/TermsOfUse.aspx

by the formation of the Zn-vacancy-Cu defect complex. As the as-grown Cu-doped ZnO sample is on the V_{Zn} line of the S-W plot, the involved defect is the complex defect containing the V_{Zn} monovacancy and Cu.

We have carried out a photoluminescence (PL) and S-W parameter studies on the ZnO films grown by the similar PLD method [42]. A defect emission peaked at 2.47 eV (a green luminescence GL) and a near band edge emission at 3.23 eV were induced in the low temperature (10 K) PL spectra after annealing at 900 ^{o}C. Moreover, VZn2 formation and Zn out-diffusion were also simultaneously observed. Temperature dependent PL study suggested that the NBE emission was associated to the combined contributions from the transitions of donor–acceptor-pair (DAP) and the free-electron-to-acceptor (FA). The GL and the NBE were thus associated to the Zn-vacancy related defect VZn2. Referring to the first principal calculated acceptor states of V_{Zn} at ε(0/-)=0.18 eV and ε(-/2-)=0.87 eV above the valance band maximum (VBM) [19], the photon energies of 2.47 eV and 3.23 eV well coincided and was thus associated respectively with the transitions from the CBM to the calculated ε(-/2-) and ε(0/-) states of V_{Zn}, although the S-W parameter data did not offer the microstructural information on the VZn2. However, the present positron lifetime measurement, which offered direct microstructural information on the Zn-vacancy related defects, showed that the VZn2 contained a divacancy structure rather than a monovacancy and thus threw doubt on the assignments of the GL and the NBE to the V_{Zn} monovacancy. One of the possibilities is that the GL may be originated from the transition from the CBM to the $V_{Zn}V_O$. This assignment has also been suggested by Li et al [43] as the photon energy of the GL was close to the transition from the CBM to the ε(+/0) of $V_{Zn}V_O$ calculated by methods based on total energies of defects in relevant charge states and energy band single particle eigenvalues [44]. However another theoretical study using the local density approximation with on-site Coulomb energy (LDA+U) and the projector augment wave potentials showed that the $V_{Zn}V_O$ divacancy had no state in the band gap [40]. Moreover, this explanation could not explain the introduction of the NBE after annealed at 900 ^{o}C. Another possible explanation is that after annealing at 900 ^{o}C V_{Zn} monovacancy is created by Zn out-diffusion. There were some V_{Zn} monovacancy though the dominant defect was divacancy formed through V_{Zn} aggregation, and the GL and NBE were associated to these V_{Zn} monovacancy. Further study is needed to clarify the origin of the GL peaked at 2.47 eV.

4. CONCLUSIONS

PAS studies revealed two kinds of Zn-vacancy related defects namely the V_{Zn} monovacancy and the $V_{Zn}V_O$ divacancy in ZnO films grown on PLD method. V_{Zn} dominated in the undoped ZnO films grown with relatively low oxygen pressure (≤1 Pa) and annealed with relatively low temperature (≤750 ^{o}C). $V_{Zn}V_O$ is favored in samples having enhanced V_{Zn} concentration through V_{Zn} aggregation. These V_{Zn} enhanced samples included the n^{+}-doped degenerate ZnO samples for which the formation of V_{Zn} is lowered, and the undoped samples annealed at 900 ^{o}C for which V_{Zn} was created by Zn out-diffusion.

ACKNOWLEDGEMENT

This work was supported by the RGC HKSAR (Project No. 17302115).

REFERENCES

[1] Ü. Özgür, Ya. I. Alivov, C. Liu, A. Teke, M. A. Reshchikov, S. Doğan, V. Avrutin, S.-J. Cho and H. Morkoç, J. Appl. Phys. **98**, 041301 (2005).

[2] S. C. Su, H. Zhu, L. X. Zhang, M. He, L. Z. Zhao, S. F. Yu, J. N. Wang, and F. C. C. Ling, Appl. Phys. Lett. **103**, 131104 (2013).

Downloaded From: https://www.spiedigitallibrary.org/conference-proceedings-of-spie on 8/16/2017 Terms of Use: https://spiedigitallibrary.spie.org/ss/TermsOfUse.aspx

[3] X. Yu, J. Ma, F. Ji, Y. Wang, X. Zhang, C. Cheng, and H. Ma, J. Cryst. Growth **274**, 474 (2005).
[4] G. A. Hirata, J. McKittrick, T. Cheeks, J. M. Siqueiros, J. A. Diaz, O. Contreras, and O.A. Lopez, Thin Solid Films **288**, 29 (1996).
[5] C. M. Pak, S. C. Su, C. C. Ling, Y. M. Lu, and D. L. Zhu, J. Phys. D: Appl. Phys. **46**, 135104 (2013).
[6] D. C. Look, Phys. Stat. Sol. B **241**, 624 (2004).
[7] V. Avrutin, D. J. Silversmith, and H. Morkoç, Proc. IEEE **98**, 1269 (2010).
[8] L. Liu, J. L. Xu, D. D. Wang, M. M. Jiang, S. P. Wang, B. H. Li, Z. Z. Zhang, D. X. Zhao, C. X. Shan, B. Yao, and D. Z. Shen, Phys. Rev. Lett. 108, 215501 (2012).
[9] J. G. Reynolds, C. L. Reynolds Jr., A. Mohanta, J. F. Muth, J. E. Rowe, H. O. Everitt, and D. E. Aspones, Appl. Phys. Lett. 102, 152114 (2013).
[10] S. Limpijumnong, S. B. Zhang, S.-H. Wei, and C. H. Park, Phys. Rev. Lett. **92**, 155504 (2004).
[11] J. C. Fan, C. Y. Zhu, S. Fung, Y. C. Zhong, K. S. Wong, Z. Xie, G. Brauer, W. Anwand, W. Skorupa, C. K. To, B. Yang, C. D. Beling, and C. C. Ling, J. Appl. Phys. **106**, 073709 (2009).
[12] D. O. Demchenko, B. Earles, H. Y. Liu, V. Avrutin, N. Izyumskaya, Ü. Özgür, and H. Morkoç, Phys. Rev. B **84**, 075201 (2011).
[13] D. C. Look, K. D. Leedy, L. Vines, B. G. Svensson, A. Zubiaga, F. Tuomisto, D. R. Boutt, and L. J. Brillson, Phys. Rev. B **84**, 115202 (2011).
[14] S. Choi, M. R. Phillips, I. Aharonovich, S. Pornsuwan, B. C. C. Cowie, and C. Ton-That, Advan. Opt. Mater. **3**, 821 (2015).
[15] K. H. Tam, C. K. Cheung, Y. H. Leung, A. B. Djurišić, C. C. Ling, C. D. Beling, S. Fung, W. M. Kwok, W. K. Chan, D. L. Phillips, L. Ding, and W. K. Ge, J. Phys. Chem. B **110**, 20865 (2006).
[16] T. S. Herng, D.-C. Qi, T. Berlijn, J. B. Yi, K. S. Yang, Y. Dai, Y. P. Feng, I. Santoso, C. Sánchez-Hanke, X. Y. Gao, A. T. S. Wee, W. Ku, J. Ding, and A. Rusydi, Phys. Rev. Lett. **105**, 207201 (2010).
[17] M. Khalid, M. Ziese, A. Setzer, P. Esquinazi, M. Lorenz, H. Hochmuth, M. Grundmann, D. Spemann, T. Butz, G. Brauer, W. Anwand, G. Fischer, W. A. Adeagbo, W. Hergert, and A. Ernst, Phys. Rev. B **80**, 035331 (2009).
[18] M. D. McCluskey and S. J. Jokela, J. Appl. Phys. **106**, 071101 (2009).
[19] A. Janotti and C. G. Van de Walle, Phys. Rev. B **76**, 165202 (2007).
[20] F. Tuomisto, V. Ranki, and K. Saarinen, Phys. Rev. Lett. **91**, 205502 (2003).
[21] E. V. Lavrov, J. Weber, F. Börrnert, C. G. Van de Walle, and R. Helbig, Phys. Rev. B **66**, 165205 (2002).
[22] G. Brauer, W. Anwand, D. Grambole, J. Grenzer, W. Skorupa, J. Čížek, J. Kuriplach, I. Procházka, C. C. Ling, C. K. So, D. Schulz, and D. Klimm, Phys. Rev. B **79**, 115212 (2009).
[23] F. Tuomisto, and I. Makkonen, Rev. Mod. Phys. **85**, 1583 (2013).
[24] *'Positron Annihilation in Semiconductors Defects Studies*', R. Krause-Rehberg and H. S. Leipner, Springer Series in Solid-State Sciencs, (Springer Verlag Berlin, 1999).
[25] F. Tuomisto, K. Saarinen, D. C. Look, and G. C. Farlow, Phys. Rev. B **72**, 085206 (2005).
[26] Z. Q. Chen, S. J. Wang, M. Maekawa, A. Kawasuso, H. Naramoto, X. L. Yuan, and T. Sekiguchi, Phys. Rev. B **75**, 245206 (2007).
[27] Z. Q. Chen, K. Betsuyaku, and A. Kawasuso, Phys. Rev. B **77**, 113204 (2008).
[28] F. A. Selim, M. H. Weber, D. Solodovnikov, and K. G. Lynn, Phys. Rev. Lett. **99**, 085502 (2007).
[29] L. W. Lu, C. K. So, C. Y. Zhu, C. J. Li, S. Fung, G. Brauer, W. Anwand, W. Skorupa and C. C. Ling, Semicond. Sci. Technol. **23**, 095028 (2008).
[30] S. Dutta, S. Chattopadhyay, D. Jana, A. Banerjee, S. Manik, S. K. Pradhan, M. Sutradhar, and A. Sarker, J. Appl. Phys. **100**, 114328 (2006).
[31] V. Venkata chalapathy, A. Galeckas, A. Zubiaga, F. Tuomisto, and A. Yu. Kuznetsov, J. Appl. Phys. **108**, 046101 (2010).
[32] A. Zubiaga, F. Tuomisto, F. Plazaola, K. Saarinen, J. A. Garcia, J. F. Rommeluere, J. Zuñiga-Pérez, and V. Muñoz-Sanjosé, Appl. Phys. Lett. **86**, 042103 (2005).
[33] S. Särkijärvi, S. Sintonen, F. Tuomisto, M. Bosund, S. Suihkonen, and H. Lipsanen, J. Crystal Growth **398**, 18 (2014).
[34] Z. Wang, S. Su, F. C. C. Ling, W. Anwand, and W. Wagner, J. Appl. Phys. **116**, 033508 (2014).

Downloaded From: https://www.spiedigitallibrary.org/conference-proceedings-of-spie on 8/16/2017 Terms of Use: https://spiedigitallibrary.spie.org/ss/TermsOfUse.aspx

[35] M. Jungmann, J. Haeberle, R. Krause-Rehberg, W. Anwand, M. Butterling, A. Wagner, J. M. Johnson and T. E. Cowan, J. Phys.: Conf. Ser. 443, 012088 (2013).
[36] A. van Veen, H. Schut, M. Clement, J. M. M. de Nijs, A. Kruseman, and M. R. IJpma, Appl. Surf. Sci. **85**, 216 (1995).
[37] K. Saarinen, T. Suski, I. Grzegory, and D. C. Look, Phys. Rev. B **64**, 233201 (2001).
[38] G. Brauer, W. Anwand, W. Skorupa, J. Kruiplach, O. Melikova, C. Moisson, H. von Wenckstern, H. Schmidt, M. Lorenz, and M. Grundmann, Phys. Rev. B **74**, 045208 (2006).
[39] S. Brummer W. Puff, A. G. Balogh, and P. Mascher, Mater. Sci. Forum **363-365,** 141 (2001).
[40] J. Bang, Y. S. Kim, C. H. Park, F Gao, and S. B. Zhang, Appl. Phys. Lett. **104**, 252101 (2014).
[41] F. C. C. Ling, Zilan Wang, L. P. Ho, M. Younas, W. Anwand, A. Wagner, S. C. Su, and C. X. Shan, Physica B **480**, 2 (2016).
[42] Zilan Wang, S. C. Su, M. Younas, F. C. C. Ling, W. Anwand, and A. Wagner, RSC Advances **5**, 12530 (2015).
[43] Mingjie Li, Guichuan Xing, Guozhong Xing, Bo Wu, Tom Wu, Xinhai Zhang, and Tse Chien Sum, Phys. Rev. B **87**, 115309 (2013).
[44] A. Chakrabarty and C. H. Patterson, J. Chem. Phys. **137**, 054709 (2012).

Downloaded From: https://www.spiedigitallibrary.org/conference-proceedings-of-spie on 8/16/2017 Terms of Use: https://spiedigitallibrary.spie.org/ss/TermsOfUse.aspx